




Improving the wear resistance of hydrophobic coating on porcelain by introducing waste porcelain particles

Xinpeng You¹, Hui Yu ^{1,2,3,*}, Lingjie Su², Jun Yin¹, Junchao Chen², Zhihui Cao², Junxi Pan², Yiting Li², Yuying Zheng², Wentao Hu²

¹*School of Biological and Environmental Engineering, Jingdezhen University, Jingdezhen 333000, China*

²*School of Materials and Chemical Engineering, Pingxiang University, Pingxiang 337055, China*

³*State Key Laboratory of Marine Resource Utilization in South China Sea, College of Materials & Chemical Engineering, Hainan University, Haikou 570228, China*

Received 6 February 2024; Received in revised form 7 April 2024; Accepted 23 May 2024

Abstract

Superhydrophobic materials have found extensive applications in everyday life and various industries due to their outstanding attributes such as waterproofing, exceptional anti-corrosion and self-cleaning capabilities. Nonetheless, their limited mechanical stability hinders their widespread use on ceramic surfaces. This study aims to address these limitations by employing industrial waste porcelain powder as a raw material and co-firing technology to create a micro-rough structure on ceramic surfaces. Furthermore, the impact of this rough structure on the wear resistance and hydrophobicity of the hydrophobic coating is investigated using the finite element method. The results indicate that the mechanical stability of the hydrophobic coating experiences a more pronounced enhancement with increasing distribution density of the micron rough structure of waste porcelain powder (WPPMRS). A dense rough structure does not only reduce its concentrated stress and improve its anti-wear ability, but also reduce the concentrated stress of hydrophobic coating to improve the protection of the coating. As a result, it substantially enhances the mechanical properties and stability of the hydrophobic coating. This work will provide valuable insights into the utilization of waste porcelain powder in sustainable superhydrophobic ceramics.

Keywords: *porcelain, sintering, hydrophobic coating, wear resistance, surfaces*

I. Introduction

Ceramics, an essential material that finds applications in power grid systems, public spaces and households, faces serious challenges originating from their inherent hydrophilic nature [1]. The hydrophilic nature of ceramic surfaces makes them prone to fog condensation and freezing particularly in damp and dusty environments [2]. This elevates the risk of pollution flashovers [3] and ice flashovers on porcelain insulators. Such incidents can cause widespread power outages, disrupting transportation, communication, industrial production, medical services and other critically important systems. Consequently, these disruptions pose a significant threat to human life, economy and overall safety [4].

In the context of daily use and building ceramics, the hydrophilic nature and susceptibility to dirt on ceramic surfaces not only create environments conducive to the growth and transmission of bacteria and viruses [5], but also impact the aesthetic appeal and cleanliness of ceramic products. Furthermore, they can result in poor product performance and a shortened lifespan.

Superhydrophobic modification technology can change the original hydrophilic properties of materials, thus endowing materials with self-cleaning, anti-fouling [6], anti-icing, anti-fogging, anti-scaling, corrosion resistance [7], drag reduction [8], oil-water separation [9] and bacteriostatic [5] characteristics. As per Raju *et al.* [10], hydrophobic modification technology has found extensive application on various surfaces including metal, fabric, paper, sponge, foam, wood and concrete. Interestingly, when applied to ceramic surfaces, this technology emerges as a universal coating method,

* Corresponding author: tel: +86 15879992948

e-mail: yh_ceramic@163.com

not limited by substrate materials. Additionally, the hydrophobic stability of this technology is notably superior when applied to concrete surfaces [11]. Application of organic materials with low surface energy onto ceramics and other substrates can render them superhydrophobic, achieving contact angles as high as 150–163°. Nonetheless, the mechanical fragility of the hydrophobic layer makes it susceptible to damage from external factors, such as friction and collisions (wind erosion, rain erosion, surface wear and rubbing during packaging and transportation), leading to a loss of its superhydrophobic properties [12].

Organic-inorganic hybrid technology [13] and primer-topcoat composite technology [14] can improve the mechanical stability of the hydrophobic layer through dispersion strengthening of nanoparticles [15] and adhesion of adhesive [16], respectively. Nevertheless, when it comes to high-strength ceramic materials subjected to specific wear conditions, the enhancement of the mechanical stability of the hydrophobic layer through these two methods falls short of meeting application standards. Rough structure construction [17] involves creating micro/nano rough structures on material surfaces, followed by modification with low surface energy to achieve superhydrophobic surfaces. This approach shifts the technical focus to the surface design of the substrate material, enabling greater control over wear resistance by manipulating the chemical composition, phase structure and microstructure of the base material. This strategy reduces the demands on the wear resistance of hydrophobic materials and enhances the mechanical and hydrophobic stability of the hydrophobic layer. As a result, it emerges as a significant method for constructing superhydrophobic surfaces [18].

Despite the continuous emergence of rough structure construction technologies, including template method [19], laser etching method [20,21], acid etching method [22,23], oxidation method [24,25], wet chemical method [26] and mechanical processing method [27]), and their ability to create specific rough structures on polymer or metal surfaces to enhance the mechanical and hydrophobic stability of the hydrophobic layer, these methods are not suitable for application in the ceramic field.

Kulkarni *et al.* [28] used pulsed laser-assisted nitriding technology to prepare an aluminium nitride composite layer with excellent mechanical properties on the surface of aluminium alloy. The surface wear is reduced by a factor of five compared to the original. Wang *et al.* [29] argued that nanoscale rough structures are too fragile to effectively facilitate the practical application of superhydrophobic surfaces. To address this limitation, they successfully developed a stepped micro-rough structure and nanopores on pure aluminium substrates through a combination of anodization and chemical etching techniques. The resulting high hardness Al_2O_3 coating, formed by anodization, imparted the sur-

face with exceptional mechanical durability, enabling resistance against water impact, grit abrasion and fabric abrasion over prolonged periods. In essence, for rigid material surfaces, nanostructures exhibit relatively weak mechanical properties and primarily serve a hydrophobic function, whereas microstructures predominantly contribute to mechanical wear resistance [17]. When the coating is worn, the constructed rigid microstructure plays a protective role similar to an “armour”, which effectively improves the mechanical wear resistance of the coating [30]. Based on the protective mechanism described above, the effectiveness of the coating’s protection is enhanced by employing a base material with higher strength and hardness, fabricated with a rough structure.

Waste porcelain powder widely comes from the production and processing of ceramic products such as daily-use porcelain, ceramic tiles, electrical insulators, etc. The worldwide production of waste porcelain powder, generated from the final polishing stages of ceramic tile manufacturing, surpasses 22 billion tons. The disposal of this waste in landfills poses significant environmental risks. Hence, enhancing the recycling of waste porcelain powder is of considerable importance. Presently, due to its outstanding mechanical properties, waste porcelain powder frequently substitutes quartz sand as an aggregate in concrete [31]. However, the research on hydrophobic modification of waste porcelain powder has not been reported. This study utilized waste porcelain powder as a material for constructing rough structures to investigate the impact of four different concentrations (2.5, 10, 17.5 and 25 wt.%) of waste porcelain powder slurry on both the wear resistance and hydrophobicity of the hydrophobic coating. Through the integration of the finite element method, the study unveiled the patterns and mechanisms underlying the influence of the distribution of waste porcelain powder micro-rough structures (WPPMRS) on the mechanical and hydrophobic properties of the hydrophobic layer. Furthermore, it identified the optimal modification approach. This work thus lays a theoretical foundation and practical directives for designing ceramic hydrophobic coatings with enhanced wear resistance.

II. Experimental

2.1. Material preparation

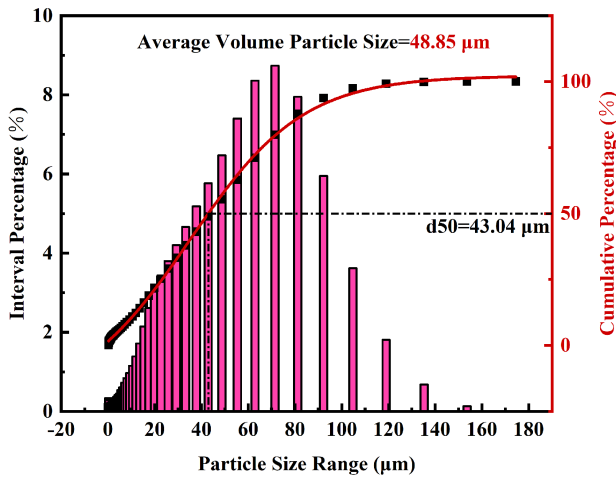
The porcelain green body and glaze of Jingdezhen Tongmen Porcelain Industry Co. Ltd. were selected to prepare ceramic sheets. The ingredients and mass ratios of the green body and glaze have been shown in Tables 1 and 2, respectively. The waste porcelain powder was purchased from Jingdezhen Baituhang Raw Materials Co. Ltd. The preparation method was as follows: the waste porcelain pieces were crushed by a jaw crusher. After passing through a 80-mesh sieve, they were ground in a horizontal ball mill at a speed of 50 rpm for 12 h with a mass ratio of the ball : powder

Table 1. Ingredients of green body

Kaolin [wt.%]	Quartz [wt.%]	Feldspar [wt.%]	Calcite [wt.%]	Talc [wt.%]
42	30	23	3	2

Table 2. Ingredients of zirconium opaque glaze

Albite [wt.%]	Quartz [wt.%]	Calcium carbonate [wt.%]	Kaolin [wt.%]	Glass powder [wt.%]	Talc [wt.%]	Zinc oxide [wt.%]	Zirconium silicate [wt.%]
29.91	23.93	16.74	9.57	5.98	2.39	2.39	9.09

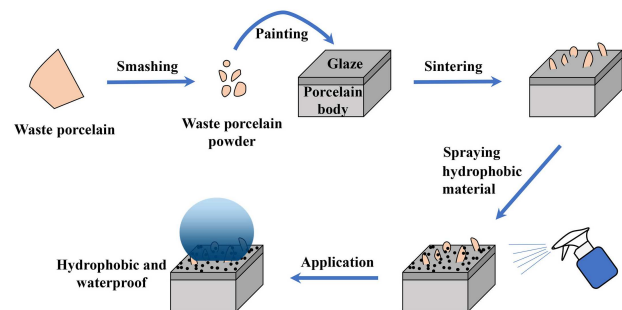
**Figure 1. Particle size distribution diagram of waste porcelain powder**

: water = 2 : 1 : 0.8, and finally dried to obtain waste porcelain powder. The particle size distribution of waste porcelain powder has been shown in Fig. 1. The average particle size of waste porcelain powder was 48.8 μm .

Polyvinyl pyrrolidone (PVP; AR; China Xilong Chemical Industry Co. Ltd.) was utilized as a dispersant for the waste porcelain powder slurry, while deionized water, produced in the laboratory, served as the solvent and dispersion medium. The PVP and deionized water were combined to create an adhesive solution with a concentration of 9.5 wt.%. Following complete dissolution using a magnetic stirrer, the prepared waste porcelain powder was sequentially added to produce waste porcelain powder slurries with concentrations of 2.5, 10, 17.5 and 25 wt.% (designated as 2.5-C, 10-C, 17.5-C, and 25-C, respectively). Subsequently, the waste porcelain powder slurry was subjected to ultrasonic dispersion for 8 min. The slurry was evenly coated on the surface of ceramic sheets by spraying method and then dried in an oven at 80 °C. The dried ceramic sheets were placed in a muffle furnace and then co-fired at 1230 °C for 30 min. The sintered ceramic sheets were cleaned and dried in the oven. To investigate the impact of waste porcelain powder micro-rough structures (WPPMRS) on hydrophobic coating effectiveness, glazed surfaces and porcelain bodies were employed as control groups.

To investigate the effect of micro-rough structures of waste porcelain powder on the hydrophobic stability of coatings, the coating 204C (from Shenzhen Weijing High-tech Material Technology Co. Ltd.) was chosen for modification. Despite its poor wear resis-

tance, this coating exhibits superhydrophobicity. Its primary constituents include fluorine-modified nano-silica (15 wt.%), silicon resin (5 wt.%) and ethanol (80 wt.%). The modified and unmodified ceramic sheets were immersed in the hydrophobic coating 204C for 10 s and then left to stand for 48 h under natural conditions. The process of preparing hydrophobic ceramics modified by waste porcelain powder is depicted in Fig. 2.

**Figure 2. The preparation process of hydrophobic ceramics modified by waste porcelain**

2.2. Characterization, modelling and analysis

Scanning electron microscope (SEM, SU8010) was used to characterize the microstructure and grain distribution of the WPPMRS prepared from slurries with different concentrations. The particle size distribution and particle spacing data were measured using Nano Measurer. The particle spacing was referred to the distance between the centres of particles. The particle size distribution of waste porcelain powder was characterized by Particle Size Distributor (Bettersize 3000).

The abrasive resistance of the WPPMRS was tested by the method of falling sand test. 15000 ml of quartz sand with a particle size of 0.7–1.85 mm was dropped freely from a stainless steel tube with a diameter of 16 mm and a height of 100 cm, and hit the sample at an inclination angle of 45°. The wear resistance of micron coating was evaluated by the attenuation of sample quality before and after wear.

Polyurethane sponge was used as wear medium, and the wear resistance of hydrophobic coating was tested by linear wear tester (Taber-5750). In the process of sample wear, the load was 100 g, the wear speed was 5 cm/s, and the wear path was 50 cm each time. The mass, contact angle and sliding angle of the sample were tested after each time of worn. The total wear was probed for 100 consecutive cycles.

The contact angle and sliding angle of each sample

after being coated with hydrophobic coating and worn were characterized by HARKE-SPCA. All values were the average of five measurements at different positions on the coating surface.

X-ray diffractometer (XRD, D8 Advance) employing Cu-K α radiation ($\lambda = 0.154$ nm) was used to characterize the phase composition of samples. The test range was 20° – 70° (2θ) with a rate of $4^\circ/\text{min}$, and step size of 0.02° .

SolidWorks was applied to model the WPPMRS coated with hydrophobic coating, and then the ANSYS static analysis module was used to calculate the stress distribution of the 3D model during abrasion process. The elasticity modulus of waste porcelain powder, wear medium and hydrophobic coating were set as 39.15 [32], 450 [33] and 0.6 GPa [34], respectively. Moreover, their Poisson's ratios were set as 0.28 [32], 0.26 [33] and 0.3 [34], respectively.

III. Results and discussion

3.1. Structure and abrasive resistance

The microstructure changes of ceramics before and after surface modification have been shown in Fig. 3. It can be seen that the surface of the unmodified glaze is very smooth, and there are no obvious pores, rough structures or surface impurity particles. This indicates that the glaze is fully melted and wetted at sintering temperature of 1230°C . The surface microstructure of the porcelain body is shown in Fig. 3b. Due to the existence of a lot of irregular crystal phases in the porcelain body, the surface presents a certain rough structure. The rough structures obtained by different concentrations of waste porcelain powder slurry are shown in Figs. 3c–f. The particle size of waste porcelain powder was about $38 \pm 16 \mu\text{m}$, which was smaller than the average parti-

cle size of $48.8 \mu\text{m}$ (Fig. 1). This phenomenon can be attributed to the irregular shape of waste porcelain powder and its deep penetration into the glaze layer during sintering, resulting in smaller particle sizes as observed in the two-dimensional image analysis. At a concentration of 2.5 wt.%, the waste porcelain powder exhibits large particle spacing, with an average powder spacing of $117 \pm 23 \mu\text{m}$. Upon increasing the concentration to 10 wt.%, the particle spacing of waste porcelain powder decreases slightly, with the average spacing reducing to $108 \pm 33 \mu\text{m}$. When the slurry concentration increased to 17.5 wt.%, the particle adhesion of waste porcelain powder increased, the particle spacing decreased substantially, and the average spacing decreased to $72 \pm 20 \mu\text{m}$. With the increase of concentration to 25 wt.%, the average particle spacing of waste porcelain powder decreased to $68 \pm 16 \mu\text{m}$. It is evident that with an increase in the concentration of waste porcelain powder, the particle distribution gradually becomes denser. However, the distribution density does not exhibit a linear increase with concentration; instead, it rises sharply between 10 and 17.5 wt.%.

Phase compositions of the waste porcelain powder and the glazes before and after modification are shown in Fig. 4. The main phases of the waste porcelain powder are quartz (PDF# 46-1045, SiO_2) and mullite (PDF# 15-0776, $\text{Al}_6\text{Si}_2\text{O}_{13}$), and the high background peak indicates the existence of glassy phase. The main phases in the zirconium opaque glaze are zircon (PDF# 06-0266, ZrSiO_4), quartz and glass phases. The primary phases present in the 17.5-C sample, resulting from co-firing waste porcelain powder and opaque glaze, consist of zirconium silicate, quartz, mullite and glass phases. Additionally, a minor quantity of cordierite (PDF# 13-0294, $\text{Mg}_2\text{Al}_4\text{Si}_5\text{O}_{18}$) is also formed. Notably, quartz [35], zircon [36], mullite [37], and cordierite [38] ex-

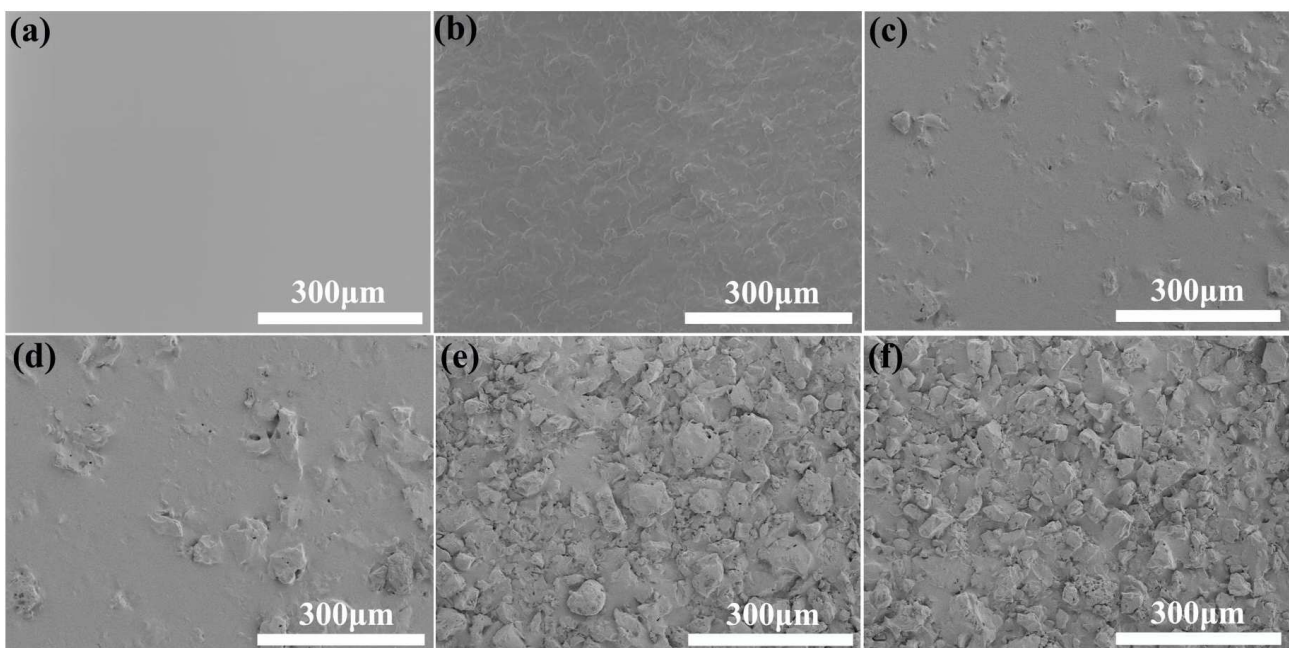


Figure 3. Surface SEM images of: a) glaze, b) porcelain body, c) 2.5-C, d) 10-C, e) 17.5-C and f) 25-C

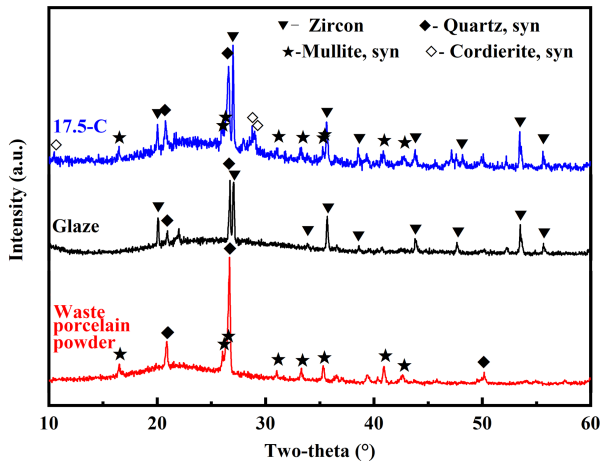


Figure 4. XRD patterns of 17.5-C sample, glaze and waste porcelain powder

hibit exceptional mechanical properties, serving as robust “armour” to safeguard hydrophobic coatings.

Figure 5 shows the abrasion rate and residual amount of the WPPMRS in the wear process. It is evident that as the concentration of waste porcelain powder increases, so does the wear rate of the constructed microstructure. This phenomenon arises because micron particles from coatings with low mass concentrations can be completely embedded within the glaze layer, resulting in firmer bonding and reduced susceptibility to the detachment during impact. Conversely, the adhesion of micron particles accumulated on the surface of high-concentration coatings is not sufficiently strong, making them more prone to the impact-induced detachment, consequently leading to a higher wear rate. Furthermore, the small effective contact area between the top of the rough structure and the wear medium increases sensitivity to the local stress overload, making it more susceptible to wear [17]. As the number of surface particles increases, the likelihood of contact between the top of the particles and falling sand significantly rises under the impact of falling sand, consequently leading to an increase in wear quality loss. The microstructure

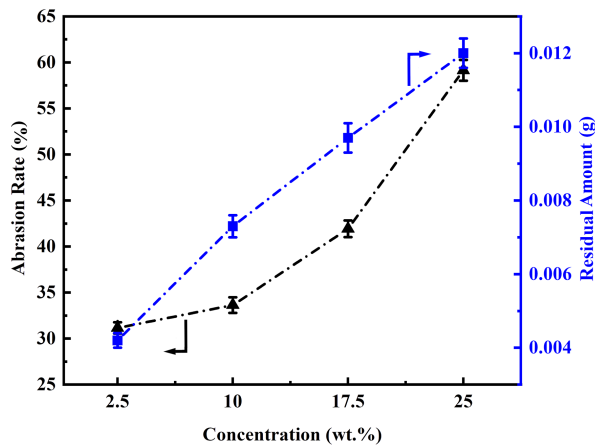


Figure 5. Abrasion rate and residual amount of 2.5-C, 10-C, 17.5-C and 25-C after 15000 ml sand falling wear

observation makes it evident that the number of waste porcelain powder particles increases gradually with the slurry concentration. Consequently, despite the nearly linear rise in wear rate, the residual amount of waste porcelain powder continues to exhibit an upward trend.

3.2. Wear resistance and hydrophobicity

Figure 6 illustrates the variation in the percentage of the residual hydrophobic layer on a smooth glazed surface, rough porcelain surface (two control groups) and four waste porcelain powder micro-rough structures (WPPMRS) during the sponge wear experiment, along with the wear rate after 100 cycles of wear. The most significant decrease in the residual percentage of the hydrophobic layer was observed for the glazed surface, followed by that on the porcelain body surface. The wear rates of the two layers after 100 cycles of wear were 76.4% and 75.0%, respectively. These very small differences in the wear rates indicate that the roughness of the porcelain surface fails to effectively protect the hydrophobic layer. The wear resistance of the hydrophobic layer, when modified with waste porcelain powder, was significantly improved. Further, as the concentration of the micron structure increases, the reduction in the mass of the hydrophobic coating slows down during wear. This suggests that higher concentrations of micron structure provide better containment and protection for the hydrophobic layer, thus enhancing the wear resistance of the sample. After 100 cycles of wear, the wear rate of coatings decreased first and then increased, and the 17.5-C sample had the lowest value of 54.2%. Nevertheless, the rise in the wear rate of the 25-C sample might be attributed to an excess of micron particles and their inadequate adhesion with the glaze layer. Consequently, these micron particles were prone to a detachment under the action of a sponge [39].

The measurements of the contact angle and sliding angle of hydrophobic coating on different microstructures during wearing are shown in Figs. 7a and 7b. Before wear, the contact angle of the hydrophobic layer modified by WPPMRS was 152–154.7°, which is higher than the 145° angle observed for the hydrophobic layer on the glazed surface and porcelain body surface. The sliding angles exhibited minimal variation, falling within the range of 0.5–1°. Throughout wear, the contact angle curve typically displays a declining trend, whereas the sliding angle curve tends to increase. Specifically, the contact angle of the hydrophobic layer on the glazed surface and porcelain surface decreased to below 90° after 5 and 10 wear cycles, respectively, indicating a shift toward hydrophilic characteristics. Additionally, their sliding angles significantly exceeded 25° after 5 wear cycles.

In the case of the 2.5-C and 10-C samples, before 40 wear cycles, the rate of decline in contact angle and the rate of increase in sliding angle for the 10-C sample were comparatively lower than those observed for the 2.5-C sample. However, after 40 wear cycles, the contact angle data for both samples were nearly aligned,

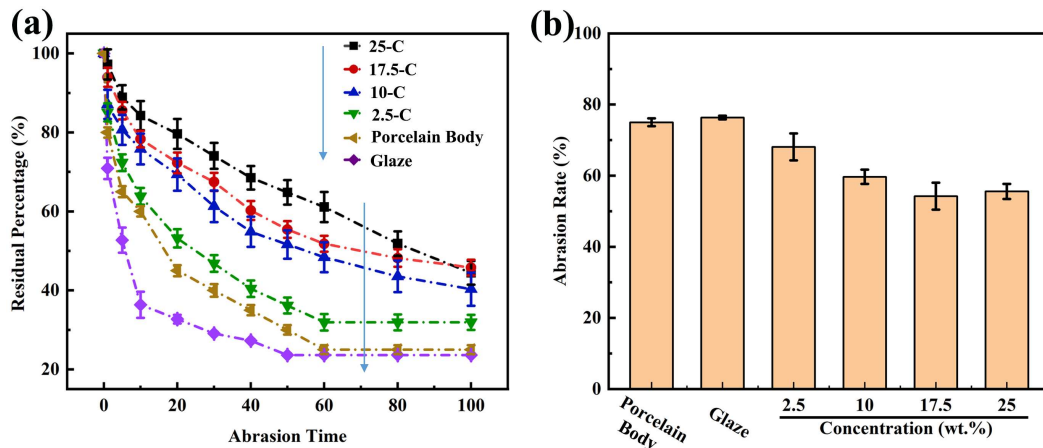


Figure 6. The residual percentage of the samples during the wear test of polyurethane sponge (a) and abrasion rate after 100 cycles of wear (b)

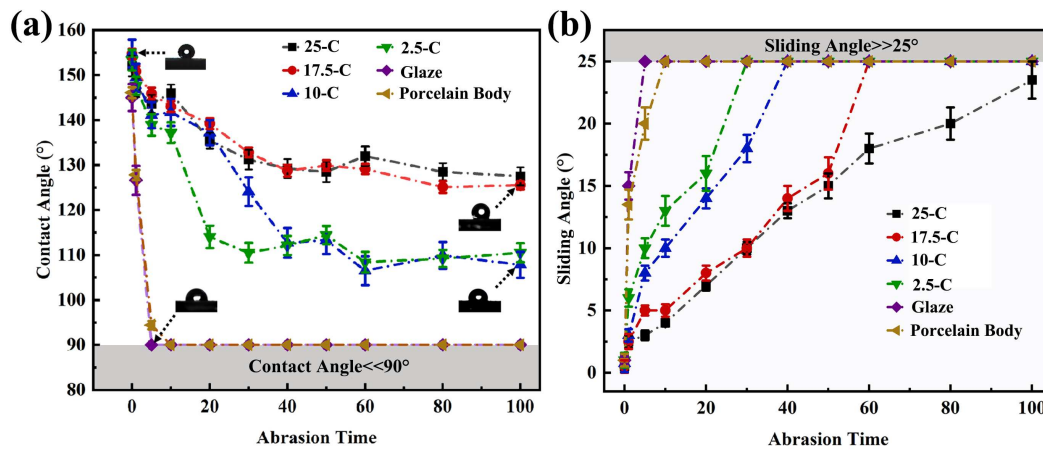


Figure 7. Contact angle (a) and sliding angle of samples during 100 cycles of polyurethane sponge abrasion (b)

and the sliding angle surpassed 25° by a significant margin. The results show that the modification effect of the 10-C structure on the hydrophobic coating was more obvious when the number of wear cycles was lower. Once the number of wear cycles reached a certain threshold, both structures underwent deterioration, and their performance disparity became less evident. The contact angle and sliding angle data for the 17.5-C and 25-C samples closely resemble each other because the distribution density of micron roughness experiences minimal alteration when the concentration reaches 17.5 wt.% or higher. As a result, this has little impact on the contact angle and sliding angle of hydrophobic coatings during wear. The properties of the 25-C and 17.5-C samples were much better than those of the 2.5-C, 10-C, and the two blank control groups. After 100 cycles of wear, the contact angles of the 25-C, 17.5-C, 10-C, 2.5-C, glaze, and porcelain body were 127.5° , 125.5° , 107.8° , 110.5° , 40.0° and 46.5° , respectively.

In the end, the 25-C sample demonstrated the best overall performance. After 100 wear cycles, the wear rate of the coating was only 55.6%, the contact angle was 127.5° , and the sliding angle was 23.5° . The coating has good mechanical and hydrophobic stability and

could be applied to self-cleaning and waterproof ceramics with high wear resistance.

In traditional bonding methods, organic [40] and inorganic [41] adhesives often cover low surface energy components, leading to a significant increase in the coating's surface energy and consequently poor superhydrophobic performance. Unlike traditional bonding methods, in this study, the micron armour formed by waste porcelain powder is affixed to the ceramic surface using glaze as an adhesive. This bonding technology solely involves adhering micron armour without covering functional hydrophobic substances. Moreover, this technique involves the bonding of ceramics and glass, typically through a mixture of covalent and ionic bonds, known for their high bonding strength [42,43], thereby ensuring the mechanical strength of the armour.

The microstructure spacing (S) has a significant influence on the freezing behaviour of supercooled droplets on superhydrophobic surfaces. Different spacing leads to three different results of droplet-substrate interaction after freezing: penetration, repulsion, and infiltration. More precisely, the penetration phenomenon mainly occurs in the microstructure with the smallest spacing ($S = 33 \mu\text{m}$). The repulsion phenomenon oc-

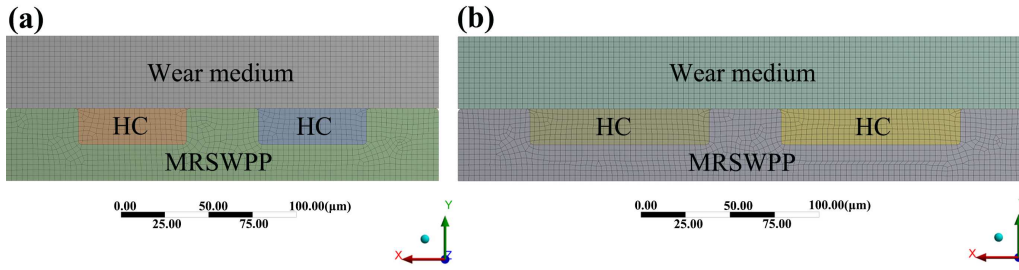


Figure 8. Meshed finite element models of 25-C (a) and 10-C (b) – HC means hydrophobic coating

curs in the microstructures with medium spacing ($S = 50 \mu\text{m}$ and $S = 56 \mu\text{m}$). Infiltration mainly occurs in micron structures with large spacing ($S \geq 70 \mu\text{m}$) [44]. Furthermore, S is also a critical geometric parameter influencing the nucleation mode of condensate droplets. A larger column spacing S promotes the formation of top and side nucleation modes, resulting in superior superhydrophobic properties. Conversely, a smaller column spacing S may lead to the bottom nucleation mode, with droplets nucleating at the corner of the array’s bottom, resulting in a Wenzel state [45]. The pitch ratio (D^*) is equal to $(R + S/2)/R$, where R is the radius of the cylindrical microstructure. A higher pitch ratio is typically associated with a larger maximum contact angle and a smaller contact angle lag, facilitating droplets to roll and bounce on the surface, thereby enhancing self-cleaning performance – a crucial parameter for designing superhydrophobic surfaces [2]. Nonetheless, the impact and mechanism of microstructure spacing on the mechanical stability of the hydrophobic functional layer remain unclear.

3.3. Finite element calculation

Finite element analysis can be used to optimize the mechanical robustness of a microstructure. The designed inverted pyramid pocket microstructure with a side wall angle α of 120° can achieve a good balance between superhydrophobicity and mechanical stability [17]. To elucidate the strengthening mechanism of the hydrophobic layer by a rough structure with high distribution density, finite element models based on the 25-C

(model 25-C) and 10-C (model 10-C) were proposed, as illustrated in Figs. 8a and 8b, respectively. Model 25-C has a spacing of $60 \mu\text{m}$ between waste porcelain powder particles, while model 10-C has a spacing of $100 \mu\text{m}$. These models simulate scenarios of a dense and a loose rough structures filled with hydrophobic coating and subsequently worn by silicon carbide sandpaper.

The stress distribution on the worn surface has been shown in Fig. 9. Under the same external force of 1 MPa, the maximum stress of hydrophobic coating in the model 25-C was 0.067 MPa, while that in the model 10-C was 0.997 MPa. Moreover, for both models, stress was concentrated in the central area of the coating surface. The findings indicate that as the particle spacing increases from 60 to $100 \mu\text{m}$, the maximum stress of the hydrophobic coating surges by 14.88 times, and the wear process commences from the centre of the coating. The maximum value of the stress on the WPPMRS of the 25-C and 10-C models was 2.002 and 2.848 MPa, respectively, with the latter registering a 42% increase compared to the former. The above results show that the dense rough structure will not only reduce the stress concentration of the hydrophobic coating to provide effective protection but also lessen the stress concentration of the rough structure itself and improve its wear resistance. This is the fundamental reason why 25-C and 17.5-C enhanced hydrophobic coatings have excellent mechanical and hydrophobic stability.

In summary, the WPPMRS demonstrates a notable enhancement in both the mechanical and hydrophobic stability of hydrophobic coatings with inadequate wear

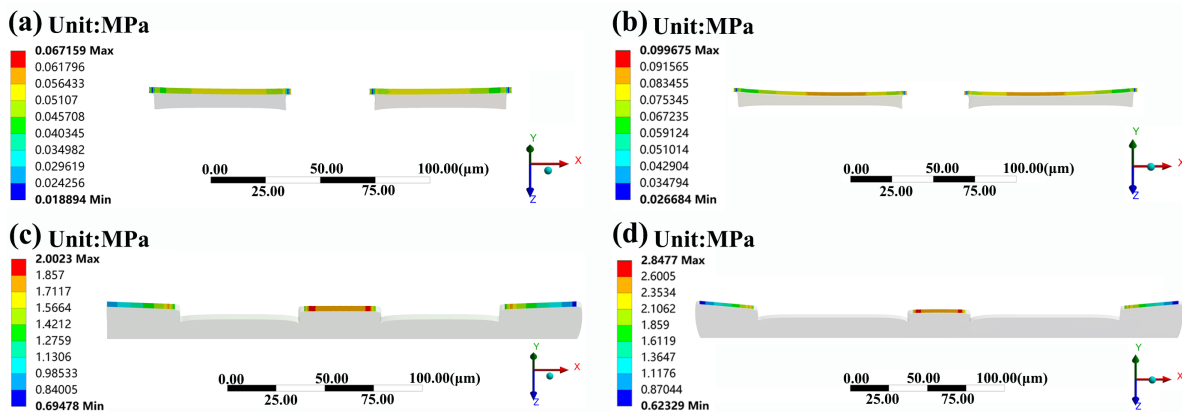


Figure 9. The stress distribution of 25-C (a) and 10-C (b) on wear surface of hydrophobic coatings, and the stress distribution of WPPMRS wear surface for 25-C (c) and 10-C (d)

resistance. Furthermore, the denser the distribution density of waste porcelain particles is, the more pronounced is the improvement effect on hydrophobic coatings. This phenomenon arises from the “armour” formed by the dense rough structure of waste porcelain powder, which not only enhances the mechanical properties of the “armour” itself but also substantially reduces the localized stress on the coatings. Consequently, it provides reliable and steady protection to the coatings.

The Cassie-Baxter composite surface is given in Eq. 1 [46]:

$$\cos \theta_{CB} = f_h \cos \theta_1 + (1 - f_h) \cos \theta_2 \quad (1)$$

where θ_{CB} is the apparent contact angle, f_h is the area fraction of the hydrophobic material (with values ranging from 0 to 1), $(1 - f_h)$ represents the area fraction of the ceramic particles, θ_1 , and θ_2 are the intrinsic contact angles of the hydrophobic material and ceramic material, respectively. The equation suggests that excessively high density of the rough structure will inevitably result in a notable decrease in f_h , consequently reducing the hydrophobicity of samples. Fortunately, this phenomenon has not occurred in this work. Nonetheless, it is a crucial factor to be considered during the hydrophobic structural design process.

IV. Conclusions

In this work, a micron rough structure was prepared on hydrophobic coatings using waste porcelain powder, and its influence on the wear resistance and hydrophobic stability of the hydrophobic coating was studied. The results demonstrate that the mechanical and hydrophobic stability of the hydrophobic layer can be simultaneously improved with the increase of waste porcelain powder micro-rough structures (WPPMRS) distribution density. When the concentration of the waste porcelain powder slurry was 25 wt.%, the hydrophobic stability was the best under the given wear conditions. After 100 cycles of wear, the contact angle of the sample was 127.5° and the sliding angle was 23.5°.

The finite element calculation results demonstrate that the increased distribution density of the WPPMRS can simultaneously decrease the concentrated stress on the hydrophobic coating and microstructure. This fundamental mechanism explains why the hydrophobic functional layers of the samples with the dense rough structure exhibit excellent wear resistance.

Employing waste porcelain powder for fabricating micron structures not only lowers the cost of raw materials but also facilitates the recycling of solid waste. This approach offers valuable insights into the cost-effective structural design of ceramic-based hydrophobic materials with high mechanical and hydrophobic stability.

Acknowledgements: The work is supported by the School-level Project of Jingdezhen University (No: 2023xjkt-04); National Natural Science Foundation

of China (No: 22265015); the National College Students Innovation and Entrepreneurship Training Program (No: 202110895003).

References

1. A. Mazumder, N. Alangi, S. Sethi, K. Prabhu, J. Mukherjee, “Study on wettability of plasma spray coated oxide ceramic for hydrophobicity”, *Surf. Interfaces*, **20** (2020) 100591.
2. A. Dhyani, J. Wang, A.K. Halvey, B. Macdonald, G. Mehta, A. Tuteja, “Design and applications of surfaces that control the accretion of matter”, *Science*, **373** [6552] (2021) 5010.
3. M. Othman, M. Isa, Z. Kása, M.N. Mazlee, M. Piah, “Effect of RTV coating on the electrical performance of porcelain insulator string under dry condition”, *IOP Conf. Ser. Mater. Sci. Eng.*, **767** (2020) 12–23.
4. Y. Hu, X. Jiang, S. Guo, R. Xian, Z. Yang, “Influence of snow accretion on arc flashover gradient for various types of insulators”, *IET Gener. Transm. Dis.*, **14** [12] (2020) 2361–2367.
5. J.J. Reinoso, E. Enriquez, V. Fuertes, “The challenge of antimicrobial glazed ceramic surfaces”, *Ceram. Int.*, **48** [6] (2022) 7393–7404.
6. Y. Ye, Z. Kang, F. Wang, Y. Long, T. Guo, D. Chen, J. Kong, L. Xu, “Achieving hierarchical structure with superhydrophobicity and enhanced anti-corrosion via electrochemical etching and chemical vapor deposition”, *Appl. Surf. Sci.*, **610** (2023) 155362.
7. K.V. Nadaraia, S.N. Suchkov, I.M. Imshinetskiy, D.V. Mashtalyar, D.Yu. Kosianov, E.A. Belov, S.L. Sinebryukhov, S.V. Gnednikov, “New superhydrophobic composite coatings on Mg-Mn-Ce magnesium alloy”, *J. Magnes. Alloys*, **11** [5] (2023) 1721–1739.
8. C. Long, X. Long, Y. Cai, X.M. Wang, C.L. Li, Y.Q. Qing, Y.L. Zhang, “Long-lived nanoparticle-embedded superhydrophobic membranes with rapid photocatalytic properties and continuous oil-water separation”, *Chem. Eng. J.*, **482** (2024) 148743.
9. P.N. Li, S.R. Wang, K. Yu, L.Y. Zhang, Y.M. Jiang, G.Q. Wang, “Superhydrophobic biomimetic microstructures prepared by laser-ablation for drag reduction”, *Colloid. Surface A*, **686** (2024) 133381.
10. A. Raju, D. Samanta, K. Rajendrakumar, “A review of recent advances in the development of superhydrophobicity over various substrate surfaces using polymers”, *ChemistrySelect*, **8** (2023) e202204262.
11. Y. Wu, W. She, D. Shi, T. Jiang, T. Hao, J. Liu, Q. Zhang, J. You, R. Li, “An extremely chemical and mechanically durable siloxane bearing copolymer coating with self-crosslinkable and anti-icing properties”, *Compos. Part. B.*, **195** (2020) 108031.
12. L.Y. Hu, X.F. Song, X.F. Zhao, F.W. Guo, F. Yang, P. Xiao, “A robust, hydrophobic CeO₂/NiCoCrAlY composite coating with excellent thermal stability and corrosion resistance prepared by air plasma spray”, *J. Alloys Compd.*, **861** (2021) 158623.
13. A. Sasidharanpillai, D. Kim, Y. Lee, G.H. Yun, Y.J. Kim, S. Lee, “Highly thermally conductive Ag/SiO₂ superhydrophobic coating for accelerated dropwise condensation”, *Ceram. Int.*, **47** [18] (2021) 26528–26538.
14. Y. Lu, S. Sathasivam, J.L. Song, C.R. Crick, C.J. Carmalt,

- I.P. Parkin, “Repellent materials. Robust self-cleaning surfaces that function when exposed to either air or oil”, *Science*, **347** (2015) 1132–1135.
15. L. Fei, Z. He, J.D. LaCoste, T.H. Nguyen, Y. Sun, “A mini review on superhydrophobic and transparent surfaces”, *Chem. Rec.*, **20** (2020) 1257–1268.
 16. W. Zhang, T. Xiang, F. Liu, M. Zhang, W. Gan, X. Zhai, X. Di, Y. Wang, G. Liu, C. Wang, “Facile design and fabrication of superwetting surfaces with excellent wear-resistance”, *ACS Appl. Mater. Inter.*, **9** [18] (2017) 15776–15784.
 17. D.H. Wang, Q.Q. Sun, M.J. Hokkanen, C.L. Zhang, F.Y. Lin, Q. Liu, S.P. Zhu, T.F. Zhou, Q. Chang, B. He, Q. Zhou, L.Q. Chen, Z.K. Wang, R.H.A. Ras, X. Deng, “Design of robust superhydrophobic surfaces”, *Nature*, **582** (2020) 55–59.
 18. J. Chen, L. Yuan, C. Shi, C. Wu, Z. Long, H. Qiao, K. Wang, Q.H. Fan, “Nature-inspired hierarchical protrusion structure construction for washable and wear-resistant superhydrophobic textiles with self-cleaning ability”, *ACS Appl. Mater. Inter.*, **13** (2021) 18142–18151.
 19. J.P. Wang, Y.L. Wu, D.G. Zhang, L. Li, T. Wang, S. Duan, “Preparation of superhydrophobic flexible tubes with water and blood repellency based on template method”, *Colloid Surface A*, **587** (2020) 124331–124336.
 20. G. Xin, C. Wu, W. Liu, Y. Rong, Y. Huang, “Anti-corrosion superhydrophobic surfaces of Al alloy based on micro-protrusion array structure fabricated by laser direct writing”, *J. Alloys Compd.*, **881** (2021) 160649.
 21. M. Ehrhardt, P. Lorenz, K. Zimmer, “Surface modification by laser etching using a surface-adsorbed layer”, *Thin Solid Films*, **520** (2012) 3629–3633.
 22. T.A. Saleh, N. Baig, “Efficient chemical etching procedure for the generation of superhydrophobic surfaces for separation of oil from water”, *Prog. Org. Coat.*, **133** (2019) 27–32.
 23. L. Ottaviano, M. Kwoka, F. Bisti, P. Parisse, V. Grossi, S. Santucci, J. Szuber, “Local surface morphology and chemistry of SnO₂ thin films deposited by rheotaxial growth and thermal oxidation method for gas sensor application”, *Thin Solid Films*, **517** [22] (2009) 6161–6169.
 24. X.H. Chen, G.B. Yang, L.H. Kong, D. Dong, L.G. Yu, J.M. Chen, P.Y. Zhang, “Direct growth of hydroxy cupric phosphate heptahydrate monocrystal with honeycomb-like porous structures on copper surface mimicking lotus leaf”, *Cryst. Growth Des.*, **9** [6] (2009) 2656–2661.
 25. Irfan, X. Wei, L. Hao, H. Lin, H. Ding, C.W. Tang, Y. Gao, “Nitric-phosphoric acid etching effects on the surface chemical composition of CdTe thin film”, *Thin Solid Films*, **520** (2012) 1988–1992.
 26. D.M. Zang, R.W. Zhu, C.X. Wu, X.G. Yu, Y. Zhang, “Fabrication of stable superhydrophobic surface with improved anticorrosion property on magnesium alloy”, *Scripta Mater.*, **69** (2013) 614–617.
 27. X.L. Yang, X. Liu, J.L. Song, J. Sun, X.H. Lu, S. Huang, F.Z. Chen, W.J. Xu, “Patterning of water traps using close-loop hydrophilic micro grooves”, *Appl. Surf. Sci.*, **389** (2016) 447–454.
 28. A.R. Kulkarni, A.K. Shukla, S.S.M. Prabu, S. Subramaniam, V.P. Balaji, I.A. Palani, M. Jayaprakash, “Investigations on enhancing the surface mechanical and tribological properties of A356 Al alloy using pulsed laser-assisted nitriding”, *Appl. Surf. Sci.*, **540** (2021) 148361.
 29. G.Y. Wang, S. Liu, S.F. Wei, Y. Liu, J.S. Lian, Q. Jiang, “Robust superhydrophobic surface on Al substrate with durability, corrosion resistance and ice-phobicity”, *Sci. Rep.*, **6** (2016) 20933.
 30. W. Cao, Z.H. Zhou, H.H. Sun, Z.J. Zhou, Y. Huang, S. Shenc, “Fabrication of abrasion-resistant micro-nano hierarchical structure on glass surface by a hydrothermal corrosion method”, *Ceram. Int.*, **48** [2] (2022) 8012–8024.
 31. A.S. El-Dieb, M.R. Taha, S.I. Abu-Eishah, “The use of ceramic waste powder (CWP) in making eco-friendly concretes”, pp. 1–35 in *Ceramic Materials - Synthesis, Characterization, Applications and Recycling*, InTech Open, Rijeka, Croatia, 2018.
 32. H. Yu, B. Zhou, L. Zhu, J.X. Yan, J.B. Li, J.L. Li, J.W. Zhang, “Mathematical law of size effect on the flexural property of ceramics”, *Ceram. Int.*, **48** (2021) 769–775.
 33. H.L. Chen, H. Jia, C.A. Zorman, P.X.L. Feng, “Determination of elastic modulus of silicon carbide (SiC) thin diaphragms via mode-dependent duffing nonlinear resonances”, *J. Microelectromech.*, **29** (2020) 783–789.
 34. L.Z. Liu, Z.Z. Ma, S.H. Pang, S.G. Zang, “Effect of polyurethane with different elastic modulus on the response of aircraft windshield against bird strike”, *Adv. Mater. Res.*, **418** (2012) 179–184.
 35. A.D.N. Junior, D. Hotza, V.C. Soler, E.S. Vilches, “Effect of quartz particle size on the mechanical behaviour of porcelain tile subjected to different cooling rates”, *J. Eur. Ceram. Soc.*, **29** [15] (2008) 1039–1046.
 36. T. Beirau, W. Oliver, C.E. Reissner, W. Nix, H. Pöllmann, R. Ewing, “Radiation-damage in multi-layered zircon: Mechanical properties”, *Appl. Phys. Lett.*, **115** [1] (2019) 081902.
 37. X.Z. Zhu, L.G. Chen, F. Zhao, J.X. Gao, K.K. Li, X.H. Liu, E.X. Xu, T.Z. Ge, L.Y. Yang, “A novel strategy to fabricate high-strength mullite by the reaction sintering method using Al³⁺/Ce⁴⁺-doped SiO₂”, *Ceram. Int.*, **47** [2] (2021) 13129–13138.
 38. M.A. Camerucci, G. Urretavizcaya, A.L. Cavalieri, “Mechanical behavior of cordierite and cordierite-mullite materials evaluated by indentation techniques”, *J. Eur. Ceram. Soc.*, **21** (2001) 1195–1204.
 39. H. Yu, Y.L. Xu, H. Chen, W.T. Hu, Y.X. Yan, J.L. Li, J.B. Li, “Enhancing the abrasion resistance of hydrophobic coatings by flower bush like micro rough structure of alumina”, *Ceram. Int.*, **48** [19] (2022) 27429–27438.
 40. J.F. Wei, J.J. Zhang, X.J. Cao, J. Huo, X. Huang, J. Zhang, “Durable superhydrophobic coatings for prevention of rain attenuation of 5G/weather radomes”, *Nat. Commun.*, **14** (2023) 2862.
 41. P. Wang, Y. Yang, H.B. Wang, H.Q. Wang, “Fabrication of super-robust and nonfluorinated superhydrophobic coating based on diatomaceous earth”, *Surf. Coat. Technol.*, **362** (2019) 90–96.
 42. A.R. Farhadzadeh, H. Ghomi, “Mechanical, structural, and thermodynamic properties of TaC-ZrC ultrahigh temperature ceramics using first principle methods”, *Mater. Res. Express*, **7** [3] (2020) 036502.
 43. R. Zhou, C. Calahoo, Y. Ding, X. Yang, L. Wondraczek, “Structural origin of the optical properties of Ag-doped fluorophosphate and sulfophosphate glasses”, *J. Phys. Chem. B*, **125** (2021) 637–656.
 44. L. Henry, G. Gustav, V. Raphael, L.C. Gaugler, B. Enea, T.M. Schutzius, P. Dimos, “Freezing-induced wetting tran-

- sitions on superhydrophobic surfaces”, *Nat. Phys.*, **19** (2023) 649–655.
45. Q. Zhang, D.K. Sun, Y.F. Zhang, M.F. Zhu, “Lattice Boltzmann modeling of droplet condensation on superhydrophobic nanoarrays”, *Langmuir*, **30** [42] (2014) 12559–12569.
46. Q.H. Zeng, H. Zhou, J.X. Huang, Z.G. Guo, “Recent development of durable superhydrophobic materials for practical applications”, *Nanoscale*, **13** (2021) 11734–11764.